

# Sensing Properties of ZnO Nanoparticles for Detection of 2-Chloroethyl Ethyl Sulfide as a Mustard Simulant

Ran Yoo<sup>1</sup>, Chihon Oh<sup>1</sup>, Min-Jung Song<sup>2</sup>, Sungmee Cho<sup>1,\*</sup>, and Wooyoung Lee<sup>1,\*</sup>

<sup>1</sup>Department of Materials Science and Engineering, Yonsei University,  
262 Seongsanno Seodaemun-gu, Seoul, 129-749, Korea

<sup>2</sup>College of Liberal Art and Interdisciplinary Studies, Kyonggi University,  
154-42 Gwanggyosan-ro, Yeongtong-gu, Suwon-si, Gyeonggi-do, 443-760, Korea

In this work, we present the fabrication and characterization of a 2-chloroethyl ethyl sulfide (2-CEES) gas sensor based on ZnO nanoparticles (NPs) synthesized by a hydrothermal method. We confirmed that synthesized ZnO NPs adopt a polycrystalline phase. Partially aggregated ZnO-NPs revealed spherical or ellipsoidal nanocrystalline particles in a size range of 30–50 nm, as observed by field-emission scanning electron microscopy (FE-SEM). The maximum response of the ZnO NPs was 15 at 1 ppm 2-CEES concentration, and a low detection limit of 0.4 ppm was observed at an optimal operating temperature of 250 °C. The lowest response time was 5.7 s in 20 ppm at 250 °C. The linearity response with correlation coefficient ( $R^2$ ) was 0.9887 at 2-CEE concentrations of 0.4–1 ppm at the operating temperature of 250 °C. The enhanced sensing performance and a decrease in the operating temperature were attributed to a high specific surface area and more active sites in the ZnO NPs after exposure to 2-CEES.

**Keywords:** ZnO Nanoparticles (NPs), Hydrothermal Method, 2-Chloroethyl Ethyl Sulfide (2-CEES), Gas Sensor.

## 1. INTRODUCTION

Weapons of mass destruction encompass chemical warfare (CW), nuclear (NW), and biological (BW) weapons. Among these, CW is possibly one of the cruelest developed by humankind because it is inexpensive and easily achieved. Chemical warfare agents (CWAs) have either lethal or incapacitating effects on humans that are used in military operations, and cause choking, bleeding, blistering, and also affect the nervous system.<sup>1</sup> Mustard gas, one of the blister agents, for example, is composed of bis(2-chloroethyl)sulfide [(CICH<sub>2</sub>CH<sub>2</sub>)<sub>2</sub>S] and 2-chloroethyl ethyl sulfide (2-CEES; C<sub>4</sub>H<sub>9</sub>ClS), and is often used as a simulant for sulfur-based mustard gas in laboratory experiments.<sup>2–4</sup> The low volatility of mustard gas means it remains in the environment and has incapacitating effects on civilian populations for a long time. Its high toxicity and imperceptibility can cause death within few minutes to few hours after exposure, depending on the gas concentration, and therefore demand

sensors with a high sensitivity and a lower limit of detection (LOD).

With increasing demands in the application of mustard gas, various metal oxide semiconductor (MOS) materials have been extensively studied for their numerous gas sensing applications. Since the applicability of MOS materials as gas sensors can be determined from their electronic structure, it is possible to choose sensing materials based on the properties of chemical species. For example, according to previously published reports, only post-transition-metal oxides with filled  $d^{10}$  cations (e.g., ZnO, SnO<sub>2</sub>, and In<sub>2</sub>O<sub>3</sub>) and transition-metal oxides with  $d^0$  (e.g., WO<sub>3</sub> and TiO<sub>2</sub>) configurations have found wide application.<sup>5</sup> Of these materials, zinc oxide (ZnO) is a promising candidate for use in gas sensors, because of its advantages such as a wide band gap (approx. 3.37 eV), chemical and thermal stability, non-toxicity, and low cost.<sup>6–8</sup> Many efforts have been attempted the development of highly sensitive and selective sensors using one dimensional (1D) to three dimensional (3D) structures.<sup>9–13</sup> This strategy provides a large surface-to-volume ratio that

\*Authors to whom correspondence should be addressed.

enables more gas diffusion and mass transport to occur in these sensors.<sup>14</sup> As for the case of gas sensors to detect CWAs, only a few groups have studied the SMO sensors using CdSnO<sub>3</sub>, Ru-CdSnO<sub>3</sub>, and Pt-doped CdSnO<sub>3</sub> thin films for 2-CEES detection,<sup>15,16</sup> and ZnO and SnO thick film sensors for DMMP detection.<sup>17</sup> However, the enhancement of the sensing properties by thin film sensors is still not satisfactory, and reliability of the sensor is needed to develop highly selective sensors to detect other reducing gases for practical use.

In this paper, we present the structural and gas sensing properties of ZnO nanoparticles (NPs) synthesized via a hydrothermal method for 2-CEES gas detection. The ZnO NPs at the sub-nanometer scale provide a high specific surface area with possibly more active sites in the presence of 2-CEES that promote rapid surface reactions, thus resulting in enhanced sensing performance.

## 2. EXPERIMENTAL DETAILS

The ZnO NPs were synthesized using a hydrothermal method.<sup>18</sup> Zinc acetate dihydrate (Zn(CH<sub>3</sub>COO)<sub>2</sub>·2H<sub>2</sub>O, Sigma-Aldrich) was first dissolved in methanol to form a 0.12 M solution, while potassium hydroxide (KOH, Sigma-Aldrich) was also dissolved in methanol to form a 0.36 M solution. The KOH solution was mixed with the zinc precursor solution under stirring at 60 °C for 24 h. Before the final sample was dried at 90 °C for 60 min, the suspension was centrifuged and washed with methanol three times. The dried samples were finally annealed at 350 °C for 30 min in a H<sub>2</sub> atmosphere, and then the resulting agglomerated ZnO powder was ground with a mortar and pestle. Prior to the fabrication of the ZnO NP-based sensor, Ti (5 nm) and Pt (150 nm) layers were deposited using a DC sputtering system on the patterned SiO<sub>2</sub> substrate. The Ti layer was used as an interlayer to provide good contact between the Pt thin film and the SiO<sub>2</sub> substrate. The synthesized powder of ZnO-NPs was mixed with  $\alpha$ -terpineol binder, which was dispersed onto the interdigitated Pt electrode. The samples were dried at 100 °C and 250 °C for 1 h, and then annealed at 600 °C for 1 h for removal of the binding agent.

Synthesized powders were structurally characterized by powder X-ray diffraction (PXRD, Ultima IV/ME 200DX, Rigaku). The size and crystalline structure were investigated by field-emission scanning electron microscopy (FE-SEM; JEOL 7001F) with energy dispersive X-ray (EDX, X Max Oxford).

For the gas sensor testing, the sensors mounted on printed circuit boards (PCB) were placed in a flow system equipped with gas cylinders and mass flow controllers (MFCs). The mixture of the 2-CEES gas and air was controlled by varying the gas flow rates produced by mass flow controllers (MFCs). Sensing properties were measured using a combination of a current source (Keithley 6220) and a nanovoltmeter (Keithley 2182) with

a constant voltage supply of 0.1 V with a time interval of 0.1 s. All of the gas-sensing measurements were conducted at the operating temperatures of 200–400 °C. The sensing response (*S*) that was calculated for the 2-CEES gas is defined by  $R_{\text{air}}S = (R_{\text{air}} - R_{\text{gas}})/R_{\text{gas}}$ , where  $R_{\text{gas}}$  and  $R_{\text{air}}$  are the resistances of the sensors in the 2-CEES containing environment and in air, respectively.<sup>19</sup> The response time and the recovery time are defined as the times required to reach 90% of total resistance change upon exposure to the test gas and to return to 10% of the original resistance in air after the test gas is released, respectively.

## 3. RESULTS AND DISCUSSION

A schematic image of an actual sensor device composed of Pt electrodes interdigitated on a SiO<sub>2</sub> substrate via a photolithography method is shown in Figure 1(a). As shown in the magnified position of the device, a ZnO NP layer is deposited on top of the Pt electrodes. Figure 1(a) on the right shows a field emission electron microscopy FE-SEM image displaying morphologies of the synthesized ZnO NPs. The ZnO NPs revealed spherical or ellipsoidal nanocrystalline particles in a size range of 30–50 nm, which were partially aggregated owing to the sintering process. Figure 1(b) shows power X-ray diffraction PXRD pattern of the synthesized ZnO NPs. An appearance of major peaks of (100), (002), and (101) in all the reflection peaks indicates a hexagonal wurtzite ZnO phase (JCPDS: # 36-1451).<sup>20</sup> No secondary phase peaks could be detected in the entire diffraction pattern.

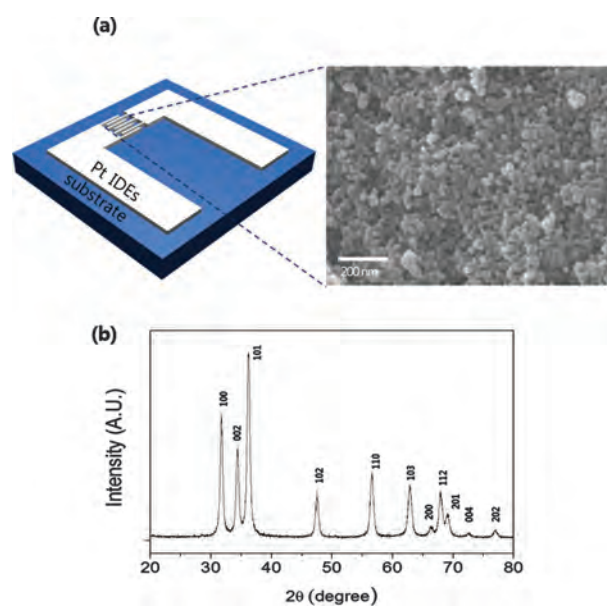


**Figure 1.** (a) A schematic drawing of an actual sensor device composed of Pt electrodes on a SiO<sub>2</sub> substrate and the scanning electron microscopy (SEM) image, and (b) powder X-ray diffraction (XRD) pattern of the ZnO NP powder.

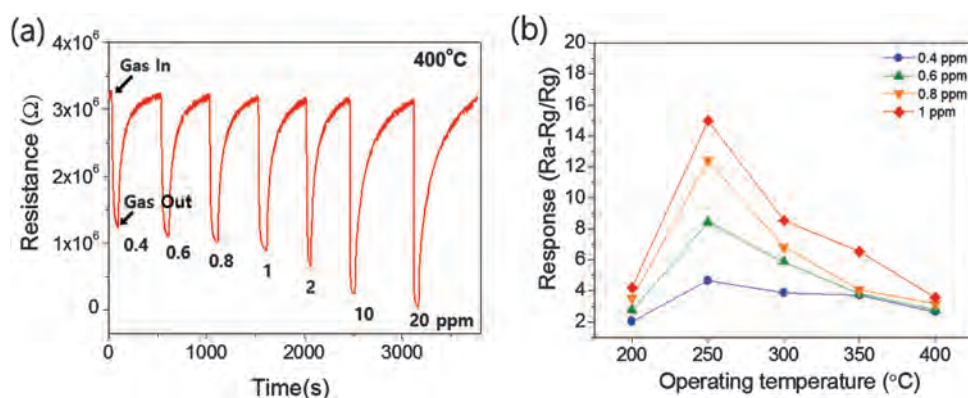


**Figure 2.** (a) Real-time resistance curves of the ZnO NPs to 2-CEES at different concentrations at 400 °C and response of the ZnO NPs to (b) different concentrations at operating temperatures of 200–400 °C in 10 ppm.

Figure 2 shows the gas sensing properties of ZnO NPs in 10 ppm 2-CEES as a function of 2-CEES concentrations and the operating temperatures. As shown in Figure 2(a), an example of a real-time resistance curve of the ZnO NPs to 2-CEES concentrations in the range of 0.4–20 ppm at an operating temperature of 400 °C. The resistance of the ZnO NPs decreased as the 2-CEES concentration increased from 0.4 to 20 ppm and the low detection limit was 0.4 ppm. The 2-CEES gas removes  $O^-$ , the concentration of which on the ZnO surface is critical to the surface reactions, and thus the resistance decreases rapidly with increasing gas concentrations. The response to various 2-CEES concentrations of 0.4–1 ppm at different operating temperatures in the range 200–400 °C was also examined, as shown in Figure 2(b). Unlike the response at 0.4 ppm, those at 0.6, 0.8, and 1 ppm show an increase up to 250 °C and then start to decrease at 300 °C. This phenomenon can be explained by a decrease in the rate of the surface chemical reaction between 2-CEES and the adsorbed surface oxygen species ( $O^{2-}$ ) of the ZnO surface 300 °C onwards. The low detection limit was 0.4 ppm over the entire temperature range, as shown in Figure 3(a). The maximum response of the ZnO-NPs was 15 in 1 ppm 2-CEES at 250 °C, which is lower than the usual operating temperatures of 300–500 °C.<sup>15,16</sup> The result indicates an optimum operating temperature of 250 °C for obtaining the highest 2-CEES sensitivity. Assuming that the ZnO NP material has sub-nanometer dimensions suggests a high specific surface area with many adsorption sites that can allow a fast chemical reaction<sup>21,22</sup> and decrease the operating temperature<sup>23</sup> when exposed to 2-CEES. More detailed sensing properties of the ZnO NPs were investigated at the optimum operating temperature of 250 °C.

Figure 3(a) presents a plot showing the response of the ZnO NPs to 2-CEES concentration in the range of 0.4–1 ppm with a linear fitting. The response shows a good linear relation at all concentrations, that is, the calibration sensitivity curve was a linear over a range from

0.4 ppm to 1 ppm, with a sensitivity of 17.5 and correlation coefficient ( $R^2$ ) of 0.9887. The response time of the ZnO NPs decreased appreciably with increasing 2-CEES concentration at 250 °C, and reached saturation at 10 ppm 2-CEES. The lowest response time was 5.7 s in 20 ppm at the same temperature, as shown in Figure 3(b). Selectivity to other target gases NO, CO, and  $NH_3$  was conducted in 10 ppm 2-CEES at 250 °C, as shown in Figure 3(c). The ZnO NPs showed a very high response of 110 for 2-CEES and low responses, in the range 15–25, for NO, CO, and  $NH_3$ .

From these results, the gas sensing mechanism of the ZnO NPs can be explained,<sup>15,16,19</sup> as described in the schematic images in Figure 4. The response of ZnO as an *n*-type metal oxide material relies on the surface chemical reaction between the adsorbed oxygen species and the target gas when exposed to 2-CEES gas. In air (Fig. 4(a)), oxygen species adsorb onto the surface of ZnO to form  $O_2^-$ ,  $O^-$  and  $O^{2-}$  ions by capturing electrons from the conduction band. The oxygen adsorption process can be represented as follows.<sup>15,16</sup>



Free electrons are transferred to the ZnO surface, forming an electron-depleted layer on the surface with a high potential barrier at the surface ( $qV_s$ ), and resulting in an increase in the resistance in the ZnO NPs. However, in 2-CEES, this target gas reacts with adsorbed species such as  $O_2^-$ ,  $O^-$ , and  $O^{2-}$  on the surface of ZnO. The two radicals formed in 2-CEES,  $ClCH_2CH_2^*$  and  $^*SCH_2CH_3$ , adsorb onto the surface of ZnO through both chlorine and sulfur moieties onto Lewis acid sites (i.e., metal ions). Oxidation of both chloroethylene and ethyl sulfide occurs after the decomposition of 2-chloroethyl ethyl sulfide as follows.<sup>15,16</sup>



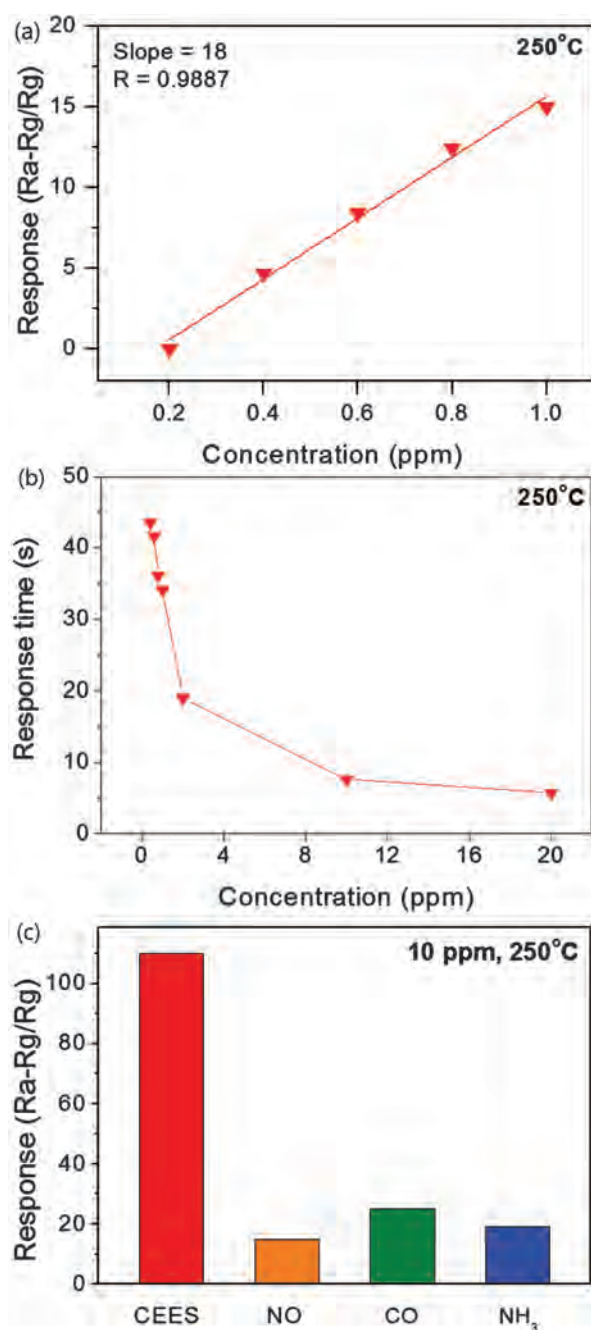
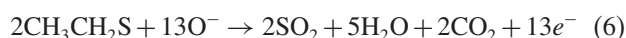


**Figure 3.** Response of the ZnO NPs (a) to 2-CEES concentrations of 0.4–1 ppm, with a linear fitting at an optimum temperature of 250 °C, (b) the response time of the ZnO NPs as a function of concentration at the operating temperature of 250 °C, and (c) selectivity of the ZnO NPs to other gases (e.g., NO, CO, and NH<sub>3</sub>) in 10 ppm at the operating temperature of 250 °C.



Finally, the electrons are released by the formation of by products such as SO<sub>2</sub>, CO<sub>2</sub>, Cl<sub>2</sub>, and H<sub>2</sub>O, and thus the thickness of the depletion layer and the resistance of the sensor decreases, as shown in Figure 4(b).

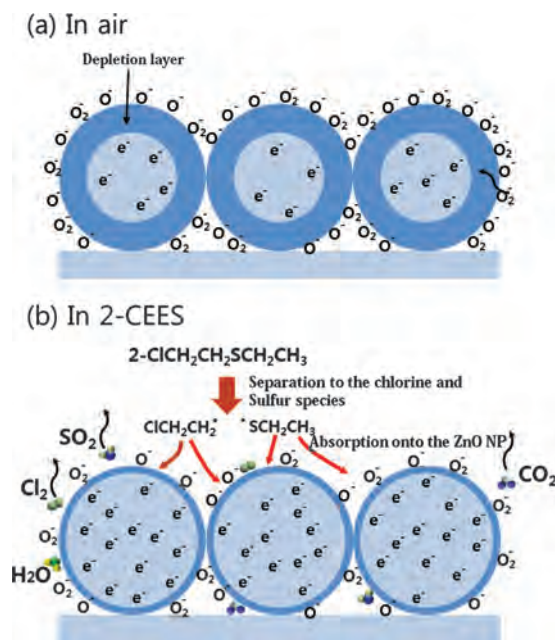


**Figure 4.** Schematic images of the sensing reaction mechanism of the ZnO NPs (a) in air and (b) in 2-CEES. In air, the oxygen molecules adsorb on the surface and take up electrons from the conduction band to form adsorbed surface oxygen species O<sub>2</sub><sup>2-</sup>, O<sub>2</sub><sup>-</sup>, and O<sup>-</sup>, leading to an increase in the thickness of the depletion layer and the resistance of the sensor. However, in 2-CEES, the surface adsorption occurs via the gas sensing reaction between 2-CEES and the adsorbed surface oxygen species of O<sub>2</sub><sup>2-</sup>, O<sub>2</sub><sup>-</sup>, and O<sup>-</sup> to form SO<sub>2</sub>, CO<sub>2</sub>, Cl<sub>2</sub>, and H<sub>2</sub>O, releases electrons, and thus reduces the thickness of the depletion layer and the sensor resistance.

#### 4. CONCLUSION

In this work, we fabricated a 2-CEES gas sensor using ZnO nanoparticles (NPs) by a hydrothermal method. Both SEM and XRD data proved that the ZnO NPs produced polycrystalline wurtzite-structured nanoparticles with uniformly sized nanoparticles in the range of 30–50 nm. The maximum response of the ZnO NPs was 15 in 1 ppm 2-CEES concentration at an optimal operating temperature of 250 °C. The calibration sensitivity was 17.5 with a correlation coefficient (*R*<sup>2</sup>) of 0.9887 at 2-CEE concentrations of 0.4–1 ppm at the operating temperature of 250 °C. The enhanced sensing performance of the ZnO NPs at 250 °C is correlated to a high surface area with more adsorption sites on the surface of the ZnO NPs.

**Acknowledgments:** This work was supported by the Agency for Defense Development through the Defense Nano Technology Application Center and Priority Research Centers Program (2009-0093823), through the National Research Foundation of Korea (NRF).

#### References and Notes

1. S. Chauhan, R. D'Cruz, S. Faruqi, K. K. Singh, S. Varma, M. Singh, and V. Karthik, *Environ. Toxicol. Pharmacol.* 26, 113 (2008).

2. S. H. Lillie, E. H. Jr, H. M. Kelly, and B. B. Rayburn, *Chemical Warfare Agents and Their Properties*, Washington DC (2005), Chap. 2, pp. 1–78.
3. R. S. Feropoulos, *Chemical Agents*, Australian DOD, Victoria (2008), pp. 2–9.
4. K. Mo and S. R. Sellevag, Norwegian Defence Research Establishment (2011), pp. 9–13.
5. G. Korotcenkov, *J. Mater. Sci.* 51, 4530 (2016).
6. J. Zhang, X. Liu, S. Wu, B. Cao, and S. Zheng, *Sens. Actuators B* 169, 61 (2012).
7. R. C. Pawar, J. S. Shaikh, S. S. Suryavanshi, and P. S. Patil, *Curr. Appl. Phys.* 12, 778 (2012).
8. T. V. Kolekar<sup>1</sup>, S. S. Bandgar, S. S. Shirguppikar, and V. S. Ganachari, *Archives of Appl. Sci. Res.* 5, 20 (2013).
9. Z. Wang, J. Gong, Y. Su, Y. Jiang, and S. Yang, *Cryst. Growth Des.* 10, 2455 (2010).
10. M. Palumbo, T. Lutz, C. E. Giusca, H. Shiozawa, V. Stolojan, D. C. Cox, R. M. Wilson, S. J. Henley, and S. R. P. Silva, *Cryst. Growth Des.* 9, 3432 (2009).
11. K. D. G. I. Jayawardena, C. Opoku, J. Fryar, S. R. P. Silva, and S. J. Henley, *Appl. Surf. Sci.* 257, 5274 (2010).
12. M. R. Alenezi, S. J. Henley, N. G. Emersona, and S. R. P. Silva, *Nanoscale* 6, 235 (2014).
13. M. McCune, W. Zhang, and Y. Deng, *Nano Lett.* 12, 3656 (2012).
14. H. S. Nalwa (ed.), *Encyclopedia of Nanoscience and Nanotechnology*, American Scientific Publishers, Los Angeles (2004), Vols. 1–10.
15. L. A. Patil, V. V. Deo, M. D. Shinde, A. R. Bari, and M. P. Kaushik, *Sens. Actuators B* 160, 234 (2011).
16. L. A. Patil, V. V. Deo, M. D. Shinde, A. R. Bari, D. M. Patil, and M. P. Kaushik, *Sens. Actuators B* 191, 130 (2014).
17. L. A. Patil, A. R. Bari, M. D. Shinde, V. Deo, and M. P. Kaushik, *Sens. Actuators B* 161, 372 (2012).
18. S. C. Lee, S. Y. Kim, W. S. Lee, S. Y. Jung, B. W. Hwang, D. Ragupathy, D. D. Lee, S. Y. Lee, and J. C. Kim, *Sens.* 11, 6893 (2011).
19. R. Yoo, S. Cho, M.-J. Song, and W. Y. Lee, *Sens.* 12, 3148 (2012).
20. B. Wang, X. Jin, Z. B. Ouyang, and P. Xu, *Appl. Phys. A* 108, 195 (2012).
21. D. K. Schroder, *Semiconductor Material and Device Characterization*, John Wiley & Sons Inc., New Jersey (2006), pp. 1–37.
22. O. Lupan, V. V. Ursaki, G. Chai, L. Chow, G. A. Emelchenko, I. M. Tiginyanu, A. N. Gruzintsev, and A. N. Redkin, *Sens. Actuators B* 144, 56 (2010).
23. B. Baruwati, D. K. Kumar, and S. V. Manorama, *Sens. Actuators B* 119, 676 (2006).

Received: 11 October 2016. Accepted: 21 November 2016.